Direct simulation of compressible wall-bounded turbulence

By Gary N. Coleman

1. Motivation and objectives

When analyzing many turbulent flows, the effects of compressibility can be neglected. Even some relatively high-speed flows, such as boundary layers generated by a supersonic aircraft, produce turbulent statistics (when scaled to account for mean density variations) that are similar to those found for the incompressible case (Bradshaw 1977). There are other situations, however, in which the nonzero divergence of the turbulence leads to behavior that is fundamentally different from that found at constant density (Speziale & Sarkar 1991). Examples include flows created by internal combustion engines, hypersonic flight, and supersonic combustion. It is with instances such as these that this project is concerned. In particular, we are interested in the effects of compressibility on turbulence near a smooth solid constant-temperature surface; our primary objective is an increased physical understanding that can be used to improve turbulence models of wall-bounded compressible flows.

With this in mind, we have begun a direct numerical simulation (DNS) study of turbulence in a plane channel. Because all of the relevant spatial and temporal scales are to be resolved, the simulations require no subgrid scale parameterization. The DNS code developed by Buell (1990, 1991) to study compressible plane Couette flow has been modified to solve the compressible Navier-Stokes equations in the plane channel. The channel was chosen over the Couette flow for two reasons: the first was to avoid using the very large streamwise domains needed to adequately capture the large Couette vortical structures (Lee 1990, Buell 1991); the second was to make use of previous experience by considering the compressible version of a well established case and isolate finite Mach number effects by comparing to the incompressible channel (Kim *et al.* 1987).

The code utilizes a Fourier-Legendre spatial discretization along with a hybrid third-order time advance algorithm developed to optimize the range of Mach numbers that may be considered (Buell 1991). The fluid is assumed to be an ideal gas, with constant specific heats and constant Prandtl number, and a (power-law) temperature dependent viscosity. Isothermal boundary conditions are used so that statistically stationary solutions may be obtained. The flow is driven by a body force rather than a mean pressure gradient to preserve streamwise homogeneity, with the body force f_i^* defined so that the bulk mass flux, $Q_* = \int_{-b_*}^{+b_*} \overline{\rho_* u_1^*} dy_*$, is constant ($y_*$ is the wall-normal coordinate, b_* the channel halfwidth, ρ_* the density, and u_1^* the streamwise velocity; "starred" quantities represent dimensional variables, and an overbar denotes an average over time and the streamwise and spanwise directions). Nondimensionalized by b_*, the bulk-averaged density $\Theta_* \equiv \frac{1}{2b_*} \int_{-b_*}^{+b_*} \overline{\rho}_* dy_*$,

the bulk velocity $\mathcal{U}_* \equiv Q_*/2b_*\Theta_*$, and the wall temperature T_w^*, the governing equations become:

$$\frac{\partial \rho}{\partial t} + \rho\frac{\partial u_j}{\partial x_j} + u_j\frac{\partial \rho}{\partial x_j} = 0, \tag{1}$$

$$\frac{\partial u_i}{\partial t} + u_j\frac{\partial u_i}{\partial x_j} + \frac{1}{\gamma M^2}\frac{\partial T}{\partial x_i} + \frac{T}{\gamma M^2 \rho}\frac{\partial \rho}{\partial x_i} - \frac{1}{Re}\frac{1}{\rho}\frac{\partial \tau_{ij}}{\partial x_j} - \Phi_i = 0, \tag{2}$$

$$\frac{\partial T}{\partial t} + u_j\frac{\partial T}{\partial x_j} + (\gamma - 1)T\frac{\partial u_j}{\partial x_j} - \frac{\gamma(\gamma-1)M_d^2}{Re}\frac{\tau_{ij}}{\rho}\frac{\partial u_i}{\partial x_j} + \frac{\gamma}{Re\ Pr}\frac{1}{\rho}\frac{\partial q_j}{\partial x_j} = 0, \tag{3}$$

$$p = \rho T/\gamma M^2, \tag{4}$$

where

$$\tau_{ij} = \mu\left(\frac{\partial u_i}{\partial x_j} + \frac{\partial u_j}{\partial x_i} - \tfrac{2}{3}\delta_{ij}\frac{\partial u_l}{\partial x_l}\right) \qquad \text{and} \qquad q_j = -\mu\frac{\partial T}{\partial x_j}.$$

The relevant nondimensional parameters are thus (a) a Mach number, $M^2 = \mathcal{U}_*^2/\gamma R_* T_w^*$; (b) a Reynolds number, $Re = \Theta_*\mathcal{U}_* b_*/\mu_w^*$; (c) the Prandtl number, $Pr = C_p^*\mu_*/k_*$; (d) the ratio of specific heats, $\gamma = C_p^*/C_v^*$; and (e) the viscosity exponent, n, where $\mu = T^n$. In the above, $\mu = \mu_*/\mu_w^*$ is the dynamic viscosity, R_* the gas constant, k_* the thermal conductivity, and the w-subscript indicates a value at the wall. Equations (1) – (4) are identical to those used by Buell (1991) except for the presence of the nondimensional forcing, $\Phi_i = b_* f_i^*/\mathcal{U}_*^2$, in (2) and the use of $\mathcal{U}_*$ in the Mach and Reynolds numbers. Another parallel to Buell (1991) is the separate Mach numbers in the momentum and energy equations, M and M_d ("d" for "dissipation"), respectively. When $M = M_d$, a "physical" simulation is obtained; when they are not equal, the results can be used to differentiate between compressibility effects associated with the pressure gradient terms in (2) and the dissipation term in (3) and thus determine the relative importance of "acoustic" and "variable-property" influences at a given Mach number. This procedure will be followed in future simulations. In the next section, preliminary results from two $M = M_d$ runs are presented.

2. Accomplishments

Two cases have been simulated, one with $M = M_d = 1.5$, the other with $M = M_d = 3$; both use $Re = 3000$, $Pr = 0.7$, $\gamma = 1.4$, and $n = 0.7$. The $M = 1.5$ run begins by superimposing small random numbers on the laminar plane-Poiseuille velocity profile and uniform density and temperature fields, while the $M = 3$ case uses a mature $M = 1.5$ field as initial conditions. (An attempt to also begin the high Mach number simulation with random numbers and laminar profiles was unsuccessful since, during the initial transient, the temperature field becomes negative and the code stops. Lower level random disturbances could be used to avoid this problem but would significantly increase the time required to obtain fully developed turbulence — and if the disturbances are too small, there is no guarantee that a turbulent state will appear. To avoid a similar high-M initialization problem, Buell

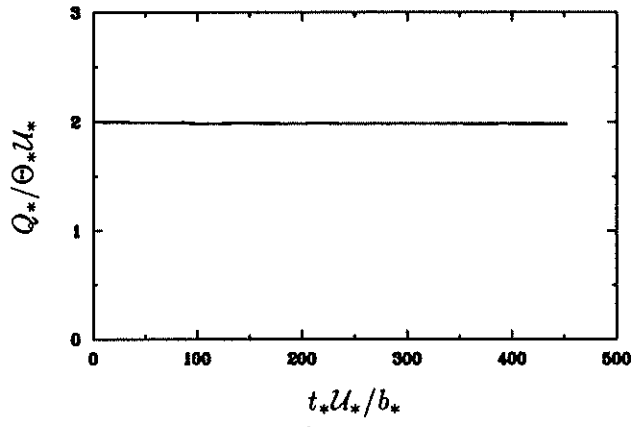

FIGURE 1. Mass flux history, $M = 1.5$ (Run m01x5g).

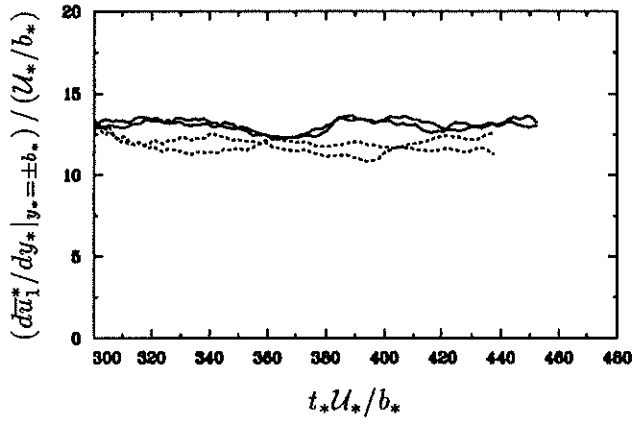

FIGURE 2. Wall shear histories at $y = \pm 1$: ——$M = 1.5$; ----$M = 3$; (Runs m01x5g and m03x0c).

(private communication) used eigenfunctions from a linear stability analysis of the Couette flow to begin his simulations.) The streamwise and spanwise domain sizes for both cases (in units of b_*) are 4π and $4\pi/3$, values that are chosen to correspond to a DNS run for the incompressible channel. The number of collocation points in the streamwise x, wall-normal y, and spanwise z directions are respectively 70, 90, and 40, which leads to the fully developed but marginally resolved turbulence desired to begin the simulations. After they have equilibrated to statistically stationary states, the flows represented by the figures below will in the future be fully resolved and studied in detail.

The $M = 1.5$ mass flux history is shown in Figure 1. To maintain the constant flux, the code adjusts the body force at each time step so that $\int_{-1}^{+1}(\partial\overline{\rho u}_1/\partial t)dy \approx \overline{\rho}\int_{-1}^{+1}(\partial\overline{u}_1/\partial t)dy = 0$ by using the Legendre quadrature routine to integrate all but

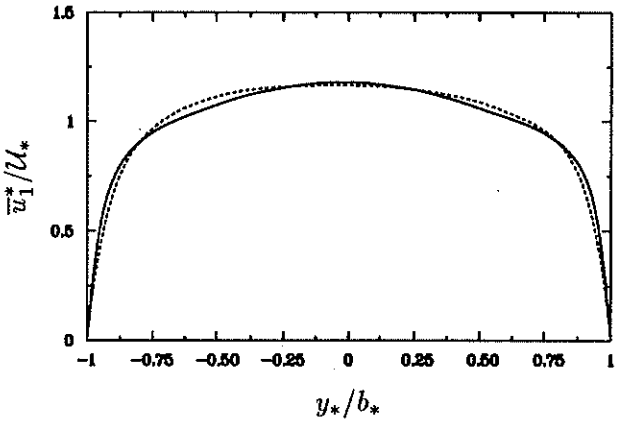

FIGURE 3. Mean streamwise velocity profiles: —— $M = 1.5$; ---- $M = 3$. Means in Figures 3–6 are the result of averaging over streamwise and spanwise directions and time; sampling period is from $t_*\mathcal{U}_*/b_* = 438$ to 448 for $M = 1.5$ and from 419 to 429 for $M = 3$.

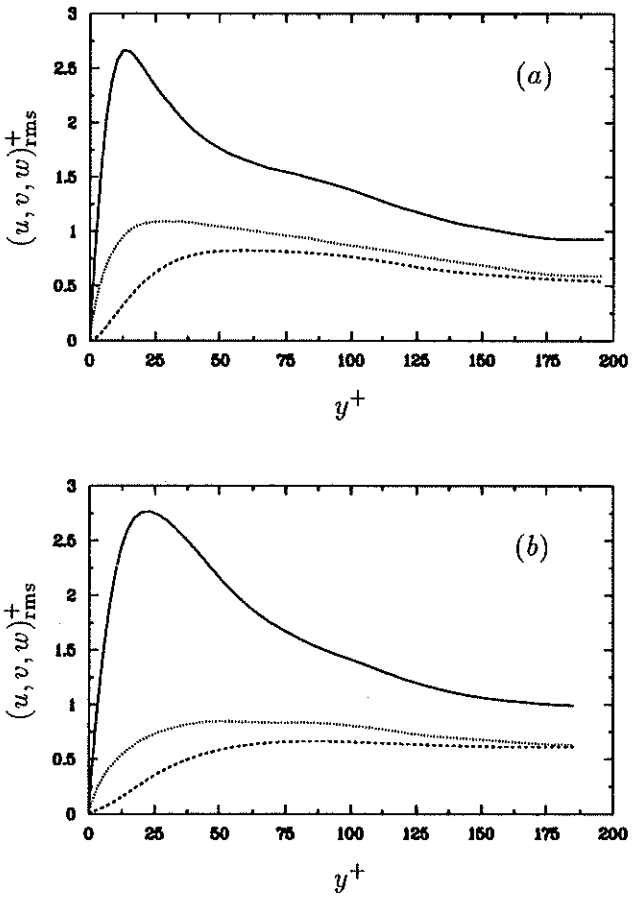

FIGURE 4. RMS velocity fluctuation profiles for (*a*) $M = 1.5$ and (*b*) $M = 3$ runs: —— streamwise; ---- wall-normal; and ····· spanwise components normalized by $(u_\tau^*)_{\rm w}$ and $\mu_{\rm w}^*/\rho_{\rm w}^*$.

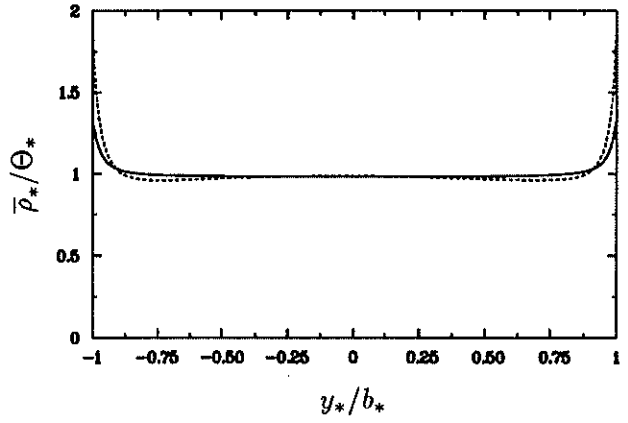

FIGURE 5. Mean density profiles: —— $M = 1.5$; ---- $M = 3$.

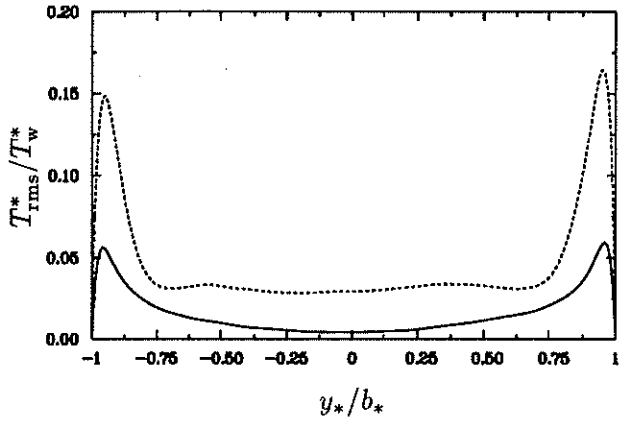

FIGURE 6. RMS temperature fluctuation profiles: —— $M = 1.5$; ---- $M = 3$.

the first and last terms in (2). Note that while this method is sufficiently accurate in practice (the value at $t = 450$ is within 1% of the initial flux), since we solve for u_i and not ρu_i, the constant-flux constraint cannot be enforced exactly.

Histories of the wall shear for the $M = 1.5$ and $M = 3$ cases are contrasted in Figure 2. As was true for the Couette DNS (Buell 1991), an increase in M leads to a drop in $|d\overline{u}_1/dy|$ at the walls. The higher Mach number is also responsible for a more pronounced flattening of the mean streamwise velocity profile as shown in Figure 3. Another similarity to the Couette results (cf. Figure 6 of Buell 1991) is revealed in Figure 4 where the near-wall maxima in the rms velocity fluctuations are observed to be less distinct at larger M. The mean density variation and temperature fluctuations are illustrated in figures 5 and 6; the large gradients of mean density (and therefore temperature) near the walls produce peaks in the rms temperature profiles, with both the density gradient and temperature fluctuations increasing with Mach number.

3. Future plans

Having modified the code and obtained preliminary results, we now intend to perform a number of case studies designed to quantify the compressibility effects. Our immediate task is to continue the $M = 1.5$ and $M = 3$ runs on a fully resolved grid and to begin new simulations for which M and M_d are not the same, as discussed above. Since there is a significant difference between the $M = 1.5$ and $M = 3$ data presented here, for the "unphysical" $M_d \neq M$ runs we will first choose $M = 3$ and $M_d = 1.5$ and then $M = 1.5$ and $M_d = 3$. Using the "$M_d \neq M$" scheme for the Couette flow, Buell (1991) found that "pure acoustic" (nonzero turbulent dilatation) effects and those due to variations of mean density are both important, with the former influencing the wall shear and the latter the large scale structures. We will determine if the same is also true for the present flow and attempt to incorporate the findings into compressible turbulence models.

REFERENCES

BRADSHAW, P. 1977 Compressible turbulent shear layers. *Ann. Rev. Fluid Mech.* **9**, 33–54.

BUELL, J. C. 1990 Direct simulations of wall-bounded compressible turbulence. In *Annual Research Briefs - 1989.* Center for Turbulence Research, Stanford Univ./NASA-Ames.

BUELL, J. C. 1991 Direct simulations of compressible wall-bounded turbulence. In *Annual Research Briefs - 1990.* Center for Turbulence Research, Stanford Univ./NASA-Ames.

KIM, J., MOIN, P. & MOSER, R. 1987 Turbulence statistics in fully developed channel flow at low Reynolds number. *J. Fluid Mech.* **177**, 133–166.

LEE, M. J. 1990 The large-scale structures in turbulent plane Couette flow. In *Annual Research Briefs - 1989.* Center for Turbulence Research, Stanford Univ./NASA-Ames.

SPEZIALE, C. G. & SARKAR, S. 1991 Second-order closure models for supersonic turbulent flows. *AIAA Paper No. 91-0212.*